energies

MDPI

Article

Wind Farm Blockage Revealed by Fog: The 2018 Horns Rev Photo Case

Charlotte Bay Hasager [1,*], Nicolai Gayle Nygaard [2] and Gregory S. Poulos [3]

[1] Department of Wind and Energy Systems, Technical University of Denmark (DTU), Frederiksborgvej 399, 4000 Roskilde, Denmark
[2] Ørsted A/S, Kraftværksvej 53, 7000 Fredericia, Denmark; nicny@orsted.com
[3] ArcVera Renewables, 1301 Arapahoe St. Ste 105, Golden, CO 80401, USA; greg.poulos@arcvera.com
* Correspondence: cbha@dtu.dk; Tel.: +45-2132-7328

Abstract: Fog conditions at the offshore wind farm Horns Rev 2 were photographed on 16 April 2018. In this study, we present the results of an analysis of the meteorological conditions on the day of the photographs. The aim of the study was to examine satellite images, meteorological observations, wind turbine data, lidar data, reanalysis data, and wake and blockage model results to assess whether wind farm blockage was a likely cause for the formation of fog upstream of the wind farm. The analysis indicated the advection of warm and moist air mass from the southwest over a cool ocean, causing cold sea fog. Wind speeds at hub height were slightly above cut-in, and there was a strong veer in the shallow stable boundary layer. The most important finding is that the wake and blockage model indicated stagnant air mass arcs to the south and west of the wind farm. In the photographs, sea fog is visible in approximately the same area. Therefore, it is likely that the reduced wind triggered the sea fog condensation due to blockage in this area. A discrepancy between the blockage model and sea fog in the photographs appears in the southwest direction. Slightly higher winds might have occurred locally in a southwesterly direction, which may have dissolved sea fog. The wake model predicted long and narrow wind turbine wakes similar to those observed in the photographs. The novelty of the study is new evidence of wind farm blockage. It fills the gap in knowledge about flow in wind farms. Implications for future research include advanced modeling of flow phenomena near large offshore wind farms relevant to wind farm operators.

Keywords: wind farm blockage; wake model; meteorological conditions; fog

Citation: Hasager, C.B.; Nygaard, N.G.; Poulos, G.S. Wind Farm Blockage Revealed by Fog: The 2018 Horns Rev Photo Case. *Energies* **2023**, *16*, 8014. https://doi.org/10.3390/en16248014

Academic Editor: Haixiao Liu

Received: 1 August 2023
Revised: 23 November 2023
Accepted: 4 December 2023
Published: 11 December 2023

1. Introduction

The current industry standard treats a wind turbine at the upstream border of a modern wind farm as if standing in isolation without further effects on the atmosphere or winds in the vicinity of the wind farm. However, recent scientific results have identified numerous impacts of a wind farm as a whole acting on the atmosphere and for considering "blockage", or combined wind farm induction zone effects, in pre-construction annual energy production (AEP) estimation. The wind farm blockage effect specifically refers to reduced wind speed well upstream of and caused by the wind farm. The reduced winds in the induction zone of upwind turbines that are part of a larger wind farm are caused by the adverse pressure gradient induced by the combined effect of the wind farm. When the wind approaches a wind farm, the atmospheric flow primarily moves through the wind farm where there are no turbines, but due to the thrust (or drag) of the turbine array, some air mass deflects upwards and over the turbine array, and some deflects to the sides of the turbine array or below the turbines. Wind farm blockage is a phenomenon that can reduce inflow wind speeds compared to the free stream winds by a substantial percentage, from a small amount to several percent. To understand the effect's magnitude and optimize wind farm design, the detailed modeling and measurement of these effects are important.

From computational fluid dynamics (CFD) simulations, it is estimated that ignoring blockage effects might give a negative bias in expected AEP [1]. In a study using an analytic vortex model to investigate blockage effects, the model results show a reduced wind speed of 2% upstream at the distance of 2.5 D, with D as the rotor diameter [2]. Comparing four engineering models and a CFD model, the reported average model blockage differences are less than 1% [3]. Furthermore, the results of large-eddy simulation (LES) show that turbine spacing is important for the blockage effect, with denser spacing causing an increase in blockage. The LES model result for neutral stratification shows a front-row power reduction of 1% at a stream-wise row separation of 7 D [4]. Extending the LES model to include atmospheric stability [5], the result shows that a stable stratified boundary layer leads to more pronounced blockage. The physical reason for this is that the deflection of cold, high-density air flowing over the wind farm creates a high-pressure region at the front of the wind farm. The resulting adverse pressure gradient increases in stable stratification with a concomitantly larger reduction in the upstream wind speed. Values of 4% front-row power reduction at a stream-wise separation of 7 D are reported [5]. The LES modeling by Strickland et al. [5] on blockage in stable stratification was performed without a capping inversion, as the model otherwise initiates gravity waves.

In case the adverse pressure gradient is as strong as in stable conditions, and the boundary layer is shallow, the wind farm blockage may trigger gravity waves [5–8]. Results from the LES model on the flow adjustment around wind farms show that thermal stratification is critical to the development of gravity waves [9]. For a weakly stratified flow, i.e., supercritical flow, the blockage extends 0.8 km upstream of the wind farm with a velocity deficit of around 1%, while for strongly stratified flow, i.e., subcritical flow, gravity waves will emerge and give a much larger, profound impact on the upwind flow, with reduced winds extending around 7 km upstream and an AEP loss of around 35% in the front-row turbines [9].

The predominant condition of concern with respect to blockage is supercritical flow. Further downstream in the far-field wake, cluster wakes prevail. For inflow wind speeds in the range from 7 m s^{-1} to rated speed, pronounced and long wind farm cluster wakes were observed from a satellite Synthetic Aperture Radar (SAR) [10,11]. Cluster wakes between neighboring large wind farms were observed to cause lower AEP at downstream wind farms [12]. SAR observations [13] and Weather Research and Forecasting (WRF) model results at wind farms and clusters in the North Sea [14] identify long wakes and blockage effects.

Although the effects were seen in wind farm power production data, atmospheric observations of wind farm blockage, particularly of its adverse pressure gradient and gravity waves or induced lift upwind, are sparse. Observing wind farm blockage is a technical challenge due to only a few percent difference between the free stream wind speed and the reduced winds in front of wind farms. Observations that have been collected to characterize and quantify blockage effects include pre- and post-construction wind data from meteorological masts and wind lidars. In some studies, the wind data were combined with turbine production data to assess the wind farm blockage. In the onshore environment, Bleeg et al. [1] used wind observations from masts pre- and post-construction near three onshore wind farms and the turbine power production to quantify the blockage effect. Their finding is, on average, a 1.9% wind speed reduction upstream at a distance of 7 to 10 D of the wind farms and 1% at a 2 km upwind distance. The results compared well with the Reynolds–Averaged Navier–Stokes (RANS) model results [1]. Blockage at another onshore wind farm was quantified by [15] from analysis of wind lidar data collected pre- and post-construction and observed at variable distances to the wind farm. The results show that blockage remains significant beyond 10 D. For daytime in unstable conditions, the wind speed reduction is 1.5% at 3 D upstream, and the model simulation result agrees with the observations [15].

In the offshore environment, observations on wind farm blockage are available. At the Lillgrund wind farm, a 2% power loss was found to originate from wind farm blockage.

The result compared actual turbine production data with expected production based on pre-construction wind resource statistics [16]. The Lillgrund wind farm production reduction due to blockage is supported using three different simulation models suggesting a 2% to 4% power loss due to wind farm blockage [16]. The turbine data analysis from the wind farm Gunfleet Sands was compared to results from a coupled engineering wake model with a simple wind farm blockage model. The results indicate an upstream area wind speed reduction and a significant variation of power among the front-row turbines [17]. The blockage effects at the Global Tech 1 wind farm were quantified using scanning wind lidar observations [18]. Reduced wind speeds of 4% over a distance of around 25 D or 2.9 km are observed for stable stratification. This result is for wind speeds in the range of high thrust when turbines operate in the partial load range. A high turbine thrust coefficient occurred from cut-in to rated wind speed, which increased the blockage effect, while for lower thrust coefficients outside this wind speed range, the blockage effect was smaller [18].

Photographs of the offshore wind farm Horns Rev 2 in foggy conditions observed on 16 April 2018 at 15:13 UTC are complementary to a case in 2008 at the Horns Rev 1 wind farm [19] and another case in 2016 at the Horns Rev 2 wind farm [20]. The photographs are fascinating due to the wind farm effects becoming visible in those particular moments where atmospheric water transforms between gaseous and liquid phases through condensation and dispersion. The transitions from water vapor to fog, and vice-versa, are governed by the moisture–temperature structure, wind speeds and wind shear, vertical motion, mixing processes, and turbulence intensity [21] that wind farms partly modify, hence triggering the exceptional fog features.

Causative factors for marine fog have different origins, but once sea fog is formed, it tends to persist due to counteracting generative and destructive processes. Advection of cooler air over a surface layer of warmer and near-saturated air and mixing of the two air masses will cause warm sea fog to form, more commonly during periods of low wind speed. In addition, long-wave radiative cooling upward from the fog will further enhance the forming of warm sea fog [21]. Advection of warm and moist air over a colder sea surface will cause cold sea fog. The cold sea fog forms in the very shallow marine layer over the sea, not up in the warm, advected air mass. The cold sea fog is a persistent, moist, and very shallow layer [21].

Warm sea fog is associated with unstable stratification, while cold sea fog is associated with stable stratification. Unstable conditions favor short and wide wakes, while stable conditions favor long and narrow wakes [22]. Wind speed, atmospheric stability, turbulence intensity, and turbine operation influence the wake development. The new photo case from 2018 shows long, narrow fog wakes similar to the case from 2016. The photo cases from 2016 and 2018 show a clearing of the fog in the far field, possibly due to the entrainment of drier air from aloft. In contrast, the case from 2008 shows short and wide fog wakes.

Compared to the previous two cases, the novelty of the 2018 case is the occurrence of sea fog located in an arc shape upwind of the wind farm; this phenomenon may be related to wind farm blockage. There is a gap in the literature on the blockage effect revealed by fog at offshore wind farms. The iconic photographs of offshore wind farm wake [19,20] are often shown in the wind industry. The new photographs might be supportive of learning about blockage effects.

The aim of our study is to investigate whether wind farm blockage is a likely cause for fog formation upstream of the wind farm. The methodology to achieve this aim is firstly a quantification of the local ambient meteorological conditions from observations, and secondly a characterization of the blockage effect on wind farms and model results from an engineering wake and blockage model simulating the conditions at the time of the photos.

The structure of the study starts with a presentation of the photographs and the wind farm in Section 2 and the ambient meteorological conditions in Section 3. Section 4 presents the results from an engineering wake model, including blockage effects and comparison to wind turbine data at the time of the photos. The Discussion and Conclusion are given in Sections 5 and 6, respectively.

2. Photographs from Horns Rev 2

The Horns Rev 2 wind farm is located in the Danish North Sea. Figure 1 shows the location. The 91 wind turbines are positioned in a curved layout. The distance between turbines in the east-to-west direction is 550 m, while the distance between turbines in the north-to-south direction varies from approximately 900 m in the west to 700 m in the east. The total distance from the southern to northern turbines is 10 km. The turbines have a 2.3 MW nameplate capacity with a rotor diameter of 93 m. The lower blade tip height is 21.5 m, and the upper blade tip height is 114.5 m above the surface. The hub height is 68 m above mean sea level (aMSL). The wind farm entered full operation in November 2009 [19]. The Horns Rev 3 wind farm (not shown) north of Horns Rev 2 was in construction and produced its first power in December 2018.

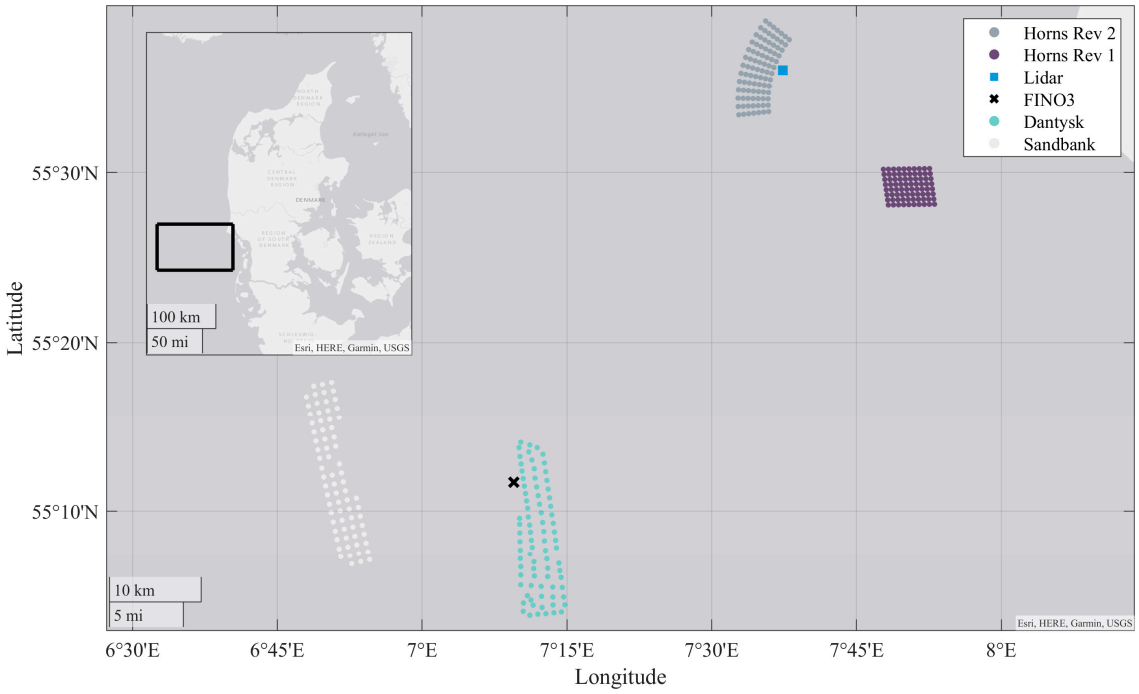

Figure 1. The black rectangle outlines the area of interest in the North Sea west of Denmark. Within the area of interest, the location of Horns Rev 1 (purple circles) and Horns Rev 2 (dark grey circles) wind farms in the Danish North Sea is shown. The blue square indicates the position of the Horns Rev 2 transformer station and lidar. The FINO3 meteorological mast is indicated by the black cross. Green and light grey circles indicate the turbines in the wind farms DanTysk and Sandbank, respectively.

The photographs were taken from a helicopter at around a 1000 m height by Henrik Krogh. The photographs from 16 April 2018 at time stamps 15:12:29, 15:12:36, 15:13:10, and 15:13:16 UTC (local time 17:12 CEST) are shown in Figure 2. At this time, the sun was at 27° elevation and sun direction 247°. The fog and turbines appear sunlit.

(**a**)

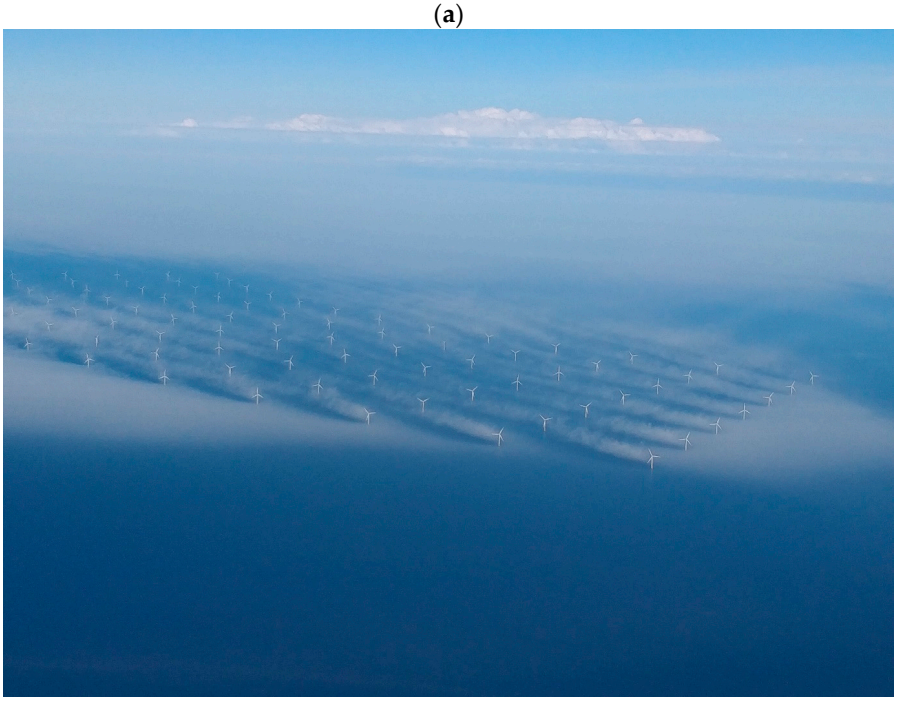

(**b**)

Figure 2. *Cont.*

(**c**)

(**d**)

Figure 2. Photograph of the Horns Rev 2 offshore wind farm on 16 April 2018 at (**a**) 15:12:29, (**b**) 15:12:36, (**c**) 15:13:10, and (**d**) 15:13:16 UTC seen from SSW direction. Copyright: Henrik Krogh.

3. Data on Meteorological Conditions

The meteorological conditions at the time of the photographs were investigated based on several data sources. The available data were the following:

- Hourly satellite observations of cloud cover from Sat24.com /Eumetsat/ Met Office [23];
- Sea surface temperature (SST) from various satellite sensors combined into a daily product by the Danish Meteorological Institute (DMI) with 0.03° horizontal resolution [24];
- Surface wind vectors observed by the ASCAT (Advanced Scatterometer) on-board the European METOP satellites from NOAA NESDIS (National Oceanic and Atmospheric

Administration, National Environmental Satellite, Data, and Information Service) observed twice per day at 25 km spatial resolution [25];

- Meteorological observations of wind speed, wind direction, air temperature, and humidity from the DMI weather station Hvide Sande at the coast of Jutland in Denmark around 50 km NE of Horns Rev at 10 min temporal resolution;
- Wind farm data at Horns Rev 2 of nacelle wind speed and produced power at 10 min temporal resolution from the supervisory control and data acquisition (SCADA) system [20];
- Wind lidar data from a WindCube V2 lidar on the deck of the transformer platform located east of the wind farm at a distance of approximately 1000 m from the nearest wind turbine (see Figure 1). It is a pulsed lidar. From the line-of-sight Doppler spectra from the four beams, the three-dimensional wind speed components were retrieved with wind speed uncertainty less than 3% [26]. The data include wind speed, wind direction, and turbulence intensity at ten vertical levels aMSL from 65.75 m to 245.75 m every 20 m, and at 68 m hub height, at 10 min temporal resolution [20];
- Wind direction and temperature measurements from the FINO3 (Forschungsplattformen in Nord- und Ostsee) meteorological mast located 52 km WSW of Horns Rev 2. Wind direction data at 29 m and 101 m and temperature readings at 29 m, 55 m, and 95 m at 10 min temporal resolution [27];
- ERA5 reanalysis data [28] sampled at the grid node closest to the Horns Rev 2 wind farm 7 km to the south. The data are hourly with 31 km horizontal resolution [29].

Air temperature, humidity, and pressure were not measured locally at Horns Rev 2 during this day.

3.1. Regional and Local Weather Conditions

The fog at the wind farm was sunlit, while a thin cloud cover was visible further east in Figure 2. This corresponds well to the thin clouds observed by satellite at 15:00 UTC in Figure 3. The cloud cover maps based on near-infrared and visual channels of the Meteosat satellite showed the clearing of the clouds from the southwest at Horns Rev [23].

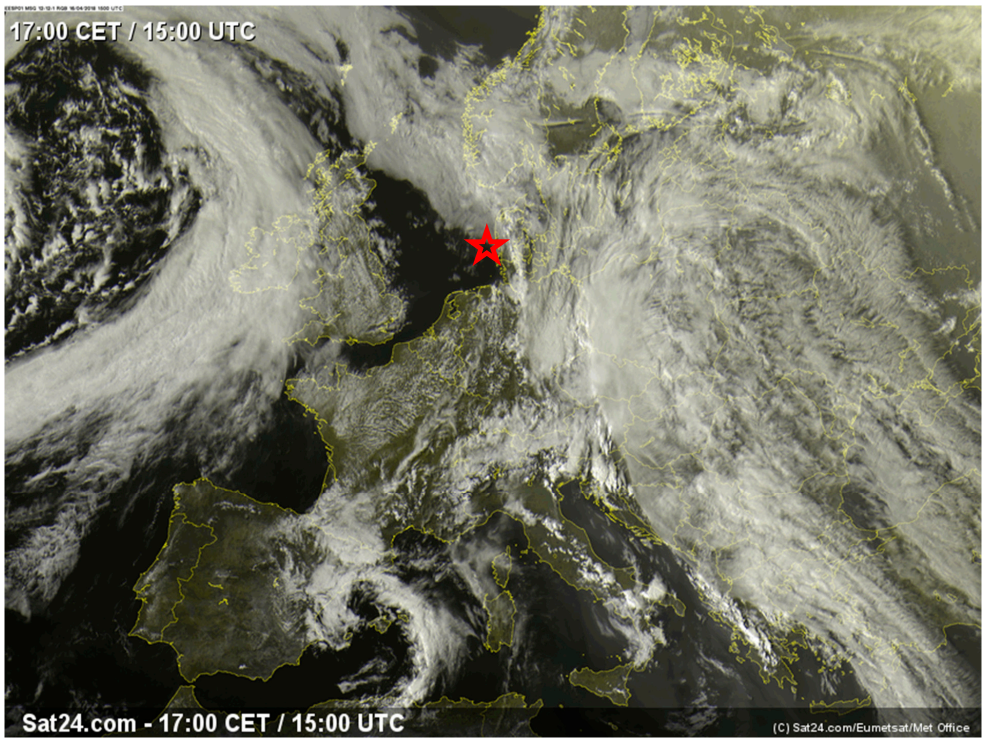

Figure 3. Cloud cover from Sat24.com/Eumetsat/Met Office on 16 April 2018 at 17:00 local time, i.e., 15:00 UTC [23]. Horns Rev is indicated with a star.

The surface winds at 10 m height above sea level were flowing from the S and SSW. At Horns Rev 2, the wind direction was 209.5°, and the wind speed was 3.8 m s^{-1}, as observed by ASCAT (Figure 4). The ASCAT surface wind data were observed at 20:58 UTC, approximately five hours after the time the photographs were taken. Wind directions were steady during the afternoon and evening, according to local data, as will be further explained in Section 3.2.

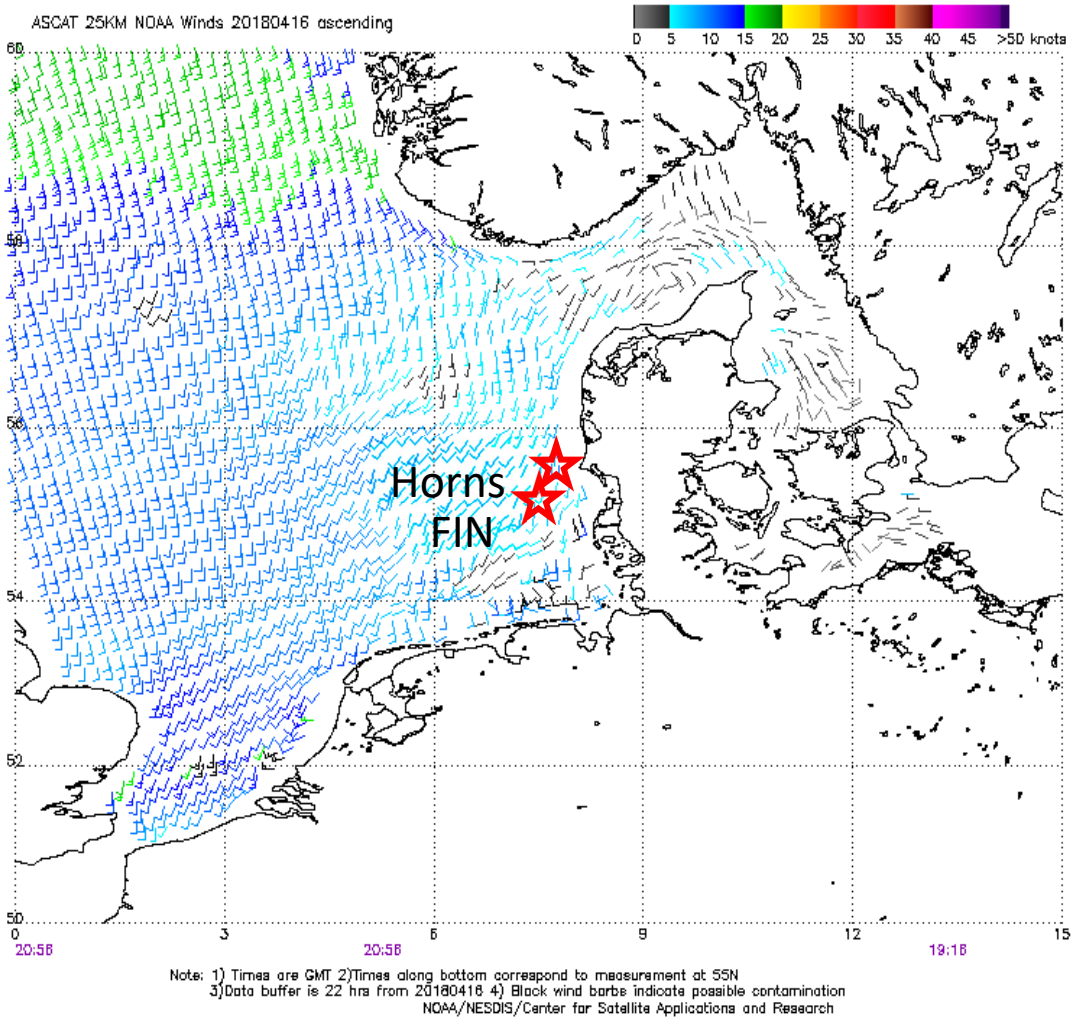

Figure 4. Ocean surface wind vector map at 10 m height based on ASCAT covering the North Sea on 16 April 2018 at 20:58 UTC [25]. Horns Rev and FINO3 are indicated with stars.

The sea surface temperature was around 4 °C at the Horns Rev 2 wind farm. The sea surface was slightly warmer towards the coast of Denmark, with sea surface temperatures up to 6 °C according to satellite observations shown in Figure 5.

Local observations of various meteorological parameters were used to characterize the atmospheric conditions at the time of the photographs. The meteorological data at Hvide Sande (see Figure 5 for the location) around 50 km NE of the wind farm show at 15:10 UTC wind speed of 5.9 m s^{-1}, wind direction 232°, air temperature 5.3 °C, wet bulb temperature 5.2 °C, dew point temperature 5.1 °C, relative humidity 99%, and no rain. These data indicate a very humid air mass and atmospheric conditions conducive to fog formation, thereby corresponding well to the observed conditions in the photographs. The air temperature was higher than the sea surface temperature (4 °C) at Horns Rev, indicating stable conditions. The wind direction was from the SW, supporting the air mass advection from this direction.

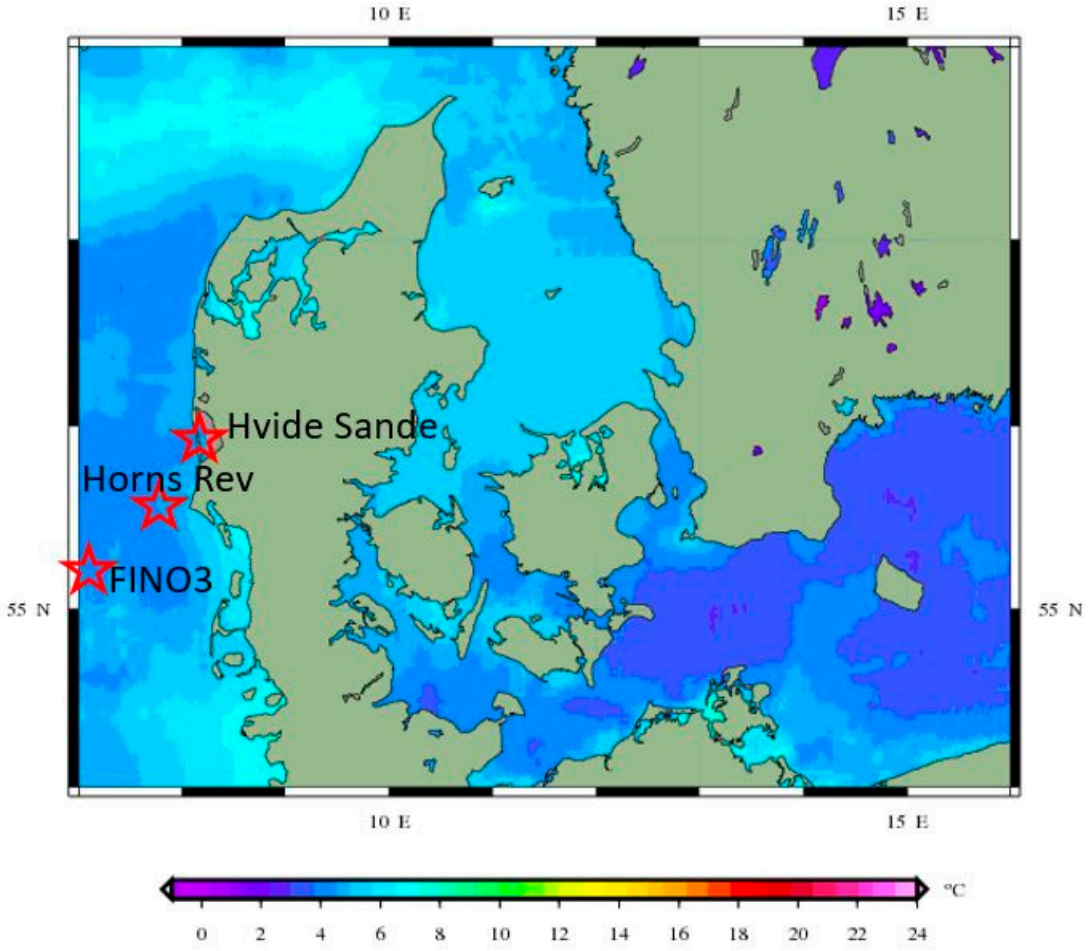

Figure 5. Average daily sea surface temperature in seas near Denmark on 16 April 2018 observed by satellites and derived by the DMI [24]. Horns Rev, FINO3, and Hvide Sande are indicated with stars.

The sea surface temperature (SST) and air temperature at 2 m from ERA5 reanalysis are shown in Figure 6, as well as air temperature observations from FINO3. The air temperature increased from around 6 °C to 7 °C in the first 100 m of the atmosphere and compares well with the air temperature observed at Hvide Sande at the time of the photographs. The sea surface temperature at 5 °C from ERA5 was slightly higher than the average daily sea surface temperature (4 °C) based on satellite data and provides further evidence of stable stratification. The relative humidity calculated from ERA5 data is 99% at 2 m, indicating condensation to fog. At FINO3, the relative humidity observed at 18 m height at the same time was 100%. Therefore, the physical observations and the reanalysis data provide evidence that humidity was high and condensation could generate cold sea fog. Fog is visible in the photographs.

At the time of the photographs, the SST from ERA5 reanalysis data was lower than the ERA5 air temperature at 2 m height, while the FINO3 observations showed warmer air aloft. This indicates stable conditions. The stable atmosphere persisted through the day, as seen in Figure 7a. Consistent with this, the Monin–Obukhov length derived from ERA5 reanalysis data was positive throughout the day, Figure 7b. The evolution of the boundary layer height, defined within the ERA5 time series, is shown in Figure 7c. The modeled boundary layer height was 180 m at 15:00 UTC, consistent with the curvature of the wind speed profile observed by the wind lidar (Figure 8) at 15:10 UTC. Boundary layers of this depth are not unusual in stable conditions over the sea.

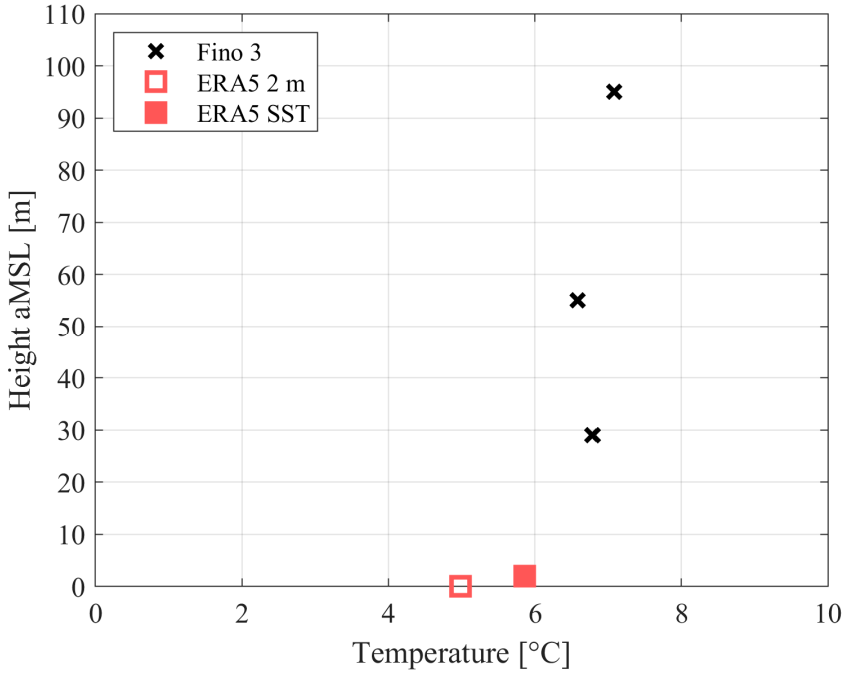

Figure 6. Sea surface temperature and 2 m air temperatures from ERA5 reanalysis data and air temperatures from FINO3 at three heights at the time of the photographs on 16 April 2018 at 15:00 UTC (ERA5 data were sampled hourly and are shown at 15:00 UTC).

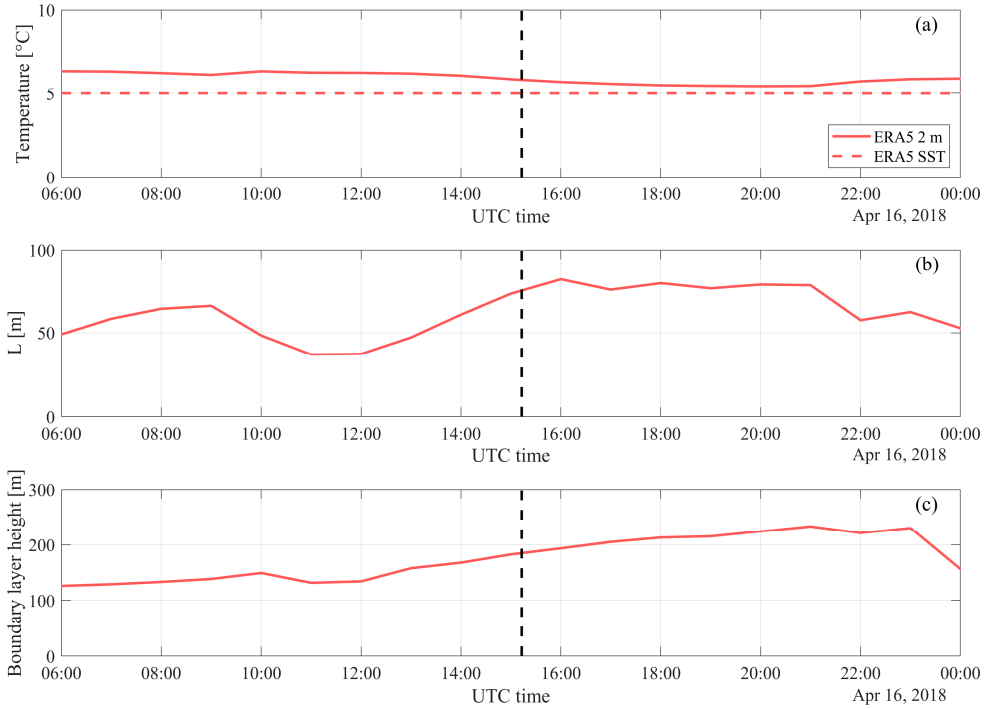

Figure 7. Time series of atmospheric variables from ERA5 reanalysis data. (**a**) Air temperature at 2 m and sea surface temperature (SST). (**b**) Monin–Obukhov length. (**c**) Boundary layer height. The time of the photographs is indicated with the dashed line.

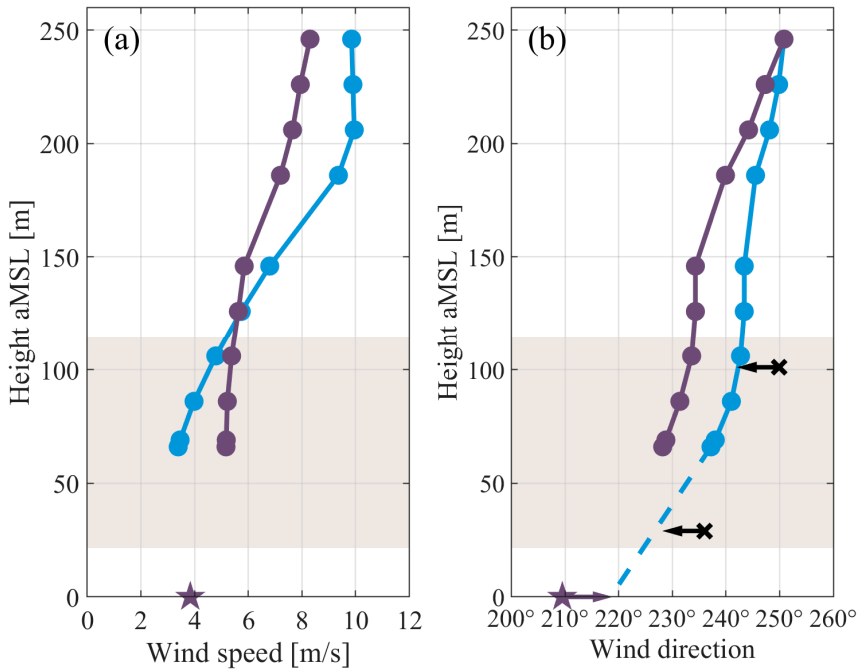

Figure 8. Observations of (**a**) mean wind speed and (**b**) wind direction above mean sea level (aMSL). Lidar observations at Horns Rev 2 on 16 April 2018 at 15:10 UTC (blue circles) and 21:00 UTC (purple circles). ASCAT observations on 16 April 2018 at 21:00 UTC (purple stars). FINO3 wind direction observations on 16 April 2018 at 15:10 UTC (black crosses). The shaded horizontal bands indicate the vertical extension of the rotor-swept area. The dashed blue line is an extrapolation of the observed wind direction towards the surface. Purple and black arrows indicate a shift of the ASCAT and FINO3 wind direction observations to the time and location of the photographs, respectively.

3.2. Wind Measurements

The wind lidar located around 1000 m east of the nearest wind turbines (Figure 1) provided observations of winds with height. Vertical profiles of wind speed and wind direction observed at 15:10 UTC are shown with the blue circles in Figure 8. It may be noted that the wind turbine wakes influenced the lidar observations at this time of day due to the southwesterly wind direction. At hub height (68 m aMSL), the waked wind speed was 3.7 m s^{-1}, and wind direction was 237° according to the lidar data. At upper blade tip height (114.5 m), the wind speed was near 5 m s^{-1}. Wind speeds increased gradually from hub height to 180 m height, indicative of boundary layer height, while from 180 m to 246 m height, wind speeds were constant at 10 m s^{-1}. The vertical wind shear, from 3.7 m s^{-1} at 68 m to 10 m s^{-1} well above the upper blade tip height, was consistent with the waking of the lidar location. The wind direction changed gradually throughout the profile. Interestingly, in the lower part of the surface layer, the wind direction changed from 237° to 243° between the 65.75 m and 108.5 m height levels; this was a wind veer of 6° over a range of 43 m height (0.14°/m). Strong veering is expected during stable atmospheric conditions.

The lowest lidar observations were at 65.75 m aMSL due to the minimum programmable measurement height and the elevation of the transformer station on which it was placed. Therefore, it is not possible to measure directly if the strong veer is present below the turbine hub height. However, surface observations from ASCAT and wind direction measurements from the bottom and top wind vanes on FINO3 substantiate the hypothesis that a strong veer was present near the surface at the time of the photographs. In Figure 8, the purple stars represent the measurements from the ASCAT overpass at 21:00 UTC. For reference, the lidar wind speed and wind direction profiles at the same time are also plotted (purple circles). The ASCAT wind direction was 209.5°, while the wind direction observed by the lidar at the lowest measurement height was 228.2° at 21:00 UTC. At 15:10 UTC, the corresponding lidar wind direction at the lowest elevation

was 237.2°. Assuming the veer in the lower atmosphere did not change between the time of the photographs and the ASCAT satellite pass, the ASCAT surface wind direction may be shifted 9° (the difference between the lowest elevation lidar wind direction measurements at the two times), giving an indicative surface wind direction of 218.5° at the time of the photographs. This shift is indicated by the purple arrow in Figure 8.

The FINO3 wind direction observations at 29 m aMSL and 101 aMSL at 15:10 UTC support this conjecture. In Figure 8b, these are marked with black crosses. The observation at 101 m is within the range of measurement heights of the lidar, and from Figure 8b, at this height, the wind direction at FINO3 was offset by 7.5° from the wind direction at Horns Rev 2. Assuming the shape of the wind direction profile was similar between the two locations for southerly flow, the same offset can be applied to shift the lower FINO3 wind direction measurement, indicating the wind direction below the lowest lidar measurement height. The shifts of the FINO3 wind direction measurements are represented by the black arrows in Figure 8b. Together, the lidar measurements and the wind direction observations from ASCAT and FINO3 are consistent with a strong veer of 0.28°/m below hub height indicated by the dashed line in Figure 8b and a surface wind direction of 218.5° at the time of the photographs.

To verify that the large difference between the lidar and ASCAT wind directions observed at 21:00 UTC does not represent a constant offset between the two data types, data from a longer period was compared at Horns Rev. Figure 9 shows the relationship between the lidar and ASCAT wind directions over three years (years 2017–2019). In general, the two wind directions are close, with ASCAT observing a slightly smaller wind direction, consistent with the modest veering of the wind direction expected under typical atmospheric conditions and significantly smaller than the severe veer observed on 16 April 2018. The results align with [30] comparing ASCAT to ferry lidar wind direction near FINO2 in the Baltic Sea. Based on the comparison results from Horns Rev, the wind direction from ASCAT is considered reliable. The assumption of strong veer in the lower part of the atmosphere is considered trustworthy.

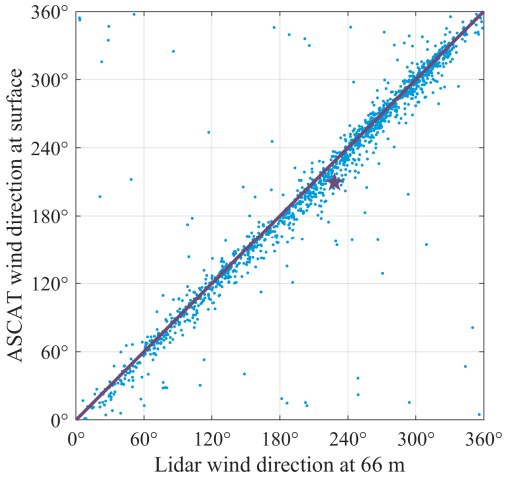

Figure 9. Correlation between the wind direction measured by the lidar and by ASCAT at Horns Rev 2 (blue dots). The purple line is the one-to-one line. The observations on 16 April 2018 at 21:00 UTC are marked with a purple star. ASCAT from ECMWF.

The temporal evolution of wind speed, wind direction, and turbulence intensity observed by the wind lidar at hub height is shown in Figure 10. Around 13:00 UTC, the wind direction changed from south to southwest such that the wind lidar was fully waked. The wind direction remained steady at around 230° after that. In the morning (6:00 to 9:00 UTC), the lidar was fully unwaked, and turbulence intensity was lower. The lidar turbulence intensity was higher and fluctuated for more than an hour after the wind direction change, possibly caused by transitional wake effects sweeping by during that time.

Thereafter, the turbulence intensity value dropped to a more stable value, approximately 2–3 times that of the unwaked morning period. In the morning, the lidar measured wind speeds around 9 to 10 m s^{-1}, dropping gradually to the waked speed around 4 m s^{-1} at 13:00 UTC and fluctuating around that value the entire afternoon.

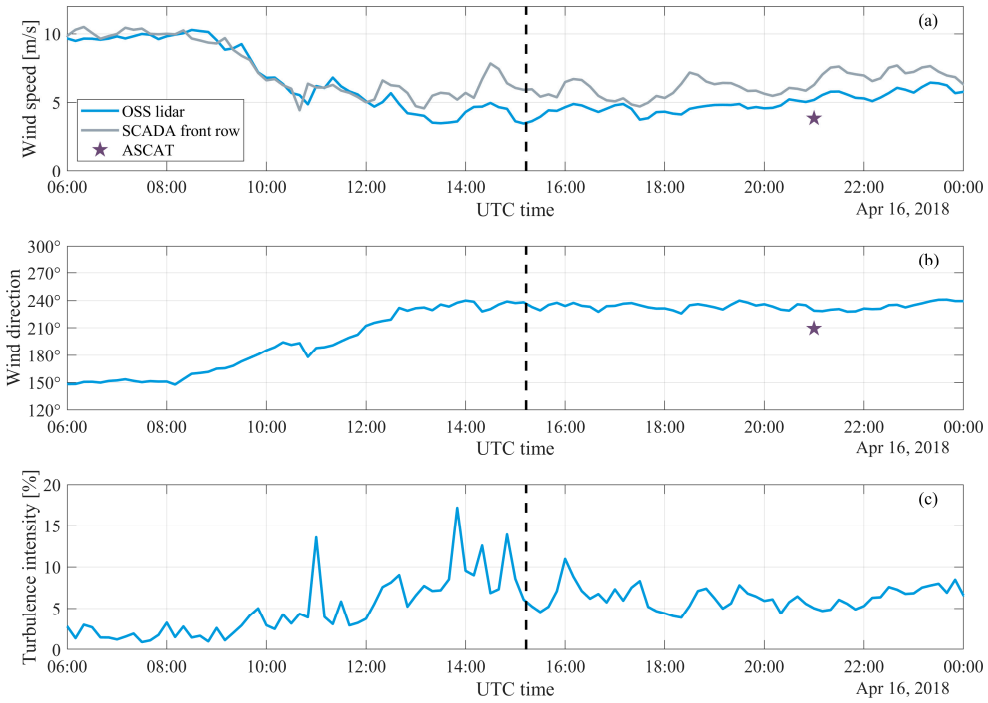

Figure 10. Time series of (**a**) wind speed, (**b**) wind direction, and (**c**) turbulence intensity observed on 16 April 2018 from the wind lidar at 68 m. Wind speed from SCADA data of front row turbines in (**a**). The ASCAT wind speed and wind direction at Horns Rev 2 are shown in (**a**,**b**). The time of the photographs is indicated with the dashed line.

The Supervisory Control And Data Acquisition (SCADA) data observed at front-row turbines also provided wind speed data. The wind speed data are shown in Figure 10a. The front row wind speeds fluctuated around 6 m s^{-1} during the afternoon, i.e., the front row wind speeds were higher than the wind speeds observed at the lidar. The fact that the lidar observed lower wind speeds at the same time is clear evidence that the lidar was awake.

At the time of the ASCAT satellite wind speed observation (around 21:00 UTC), the front row wind speed at hub height was around 7 m s^{-1}, while the satellite showed around 6 m s^{-1} at 10 m height.

In summary, the data analysis indicates stable stratification within a shallow boundary layer, near 6 m s^{-1} unwaked wind speeds from SW at hub height with wind shear to 180 m, relative humidity approaching 100%, and significant wind veer. In combination, these conditions are consistent with those required for condensation when sufficient mixing or lift is present and cold sea fog.

4. Modelling the Wake Deficit and Blockage Effect

The wake deficit and blockage effect were modeled at the time of the photos with the coupled engineering models for wind farm wake and blockage effect as presented in [17]. The wake model predicts the downstream conditions, while the blockage model predicts the upstream conditions. The thrust coefficient of every turbine from the wake model was input to the blockage model. The blockage from other wind turbines changes the incoming wind; thus, an iterative calculation was performed. In this way, a coupling between the wake and blockage models was done. The blockage model includes the accumulation of single-turbine induction effects described by a potential flow model. The

results obtained with the coupled models were based on input wind direction from the wind lidar measurement at hub height, while the input wind speed was derived from the unwaked front-row turbines.

The wake model predicted long and narrow turbine wakes (Figure 11a). This is also observed in the photos. However, there is a difference in the directional alignment of the turbine wakes between the model results and the photos. According to the engineering model, straight wakes were predicted, while in the photographs, a slight clockwise curving is noticed. The wind veer was 0.14°/m in the upper swept area. Based on surface observations from ASCAT and measurements from FINO3, the veer in the lower part of the rotor swept area is believed to be even stronger. In strong veer, the turbine wakes turn clockwise [31]. The model does not resolve the veer, but for comparison, the model output using an inflow wind direction of 219° estimated near the surface is shown in Figure 11c. The orientation of the resulting wake pattern matches the fog trails in the photographs better. The agreement with the observed pattern of production is slightly better when the wake simulation is based on the observed wind direction at hub height.

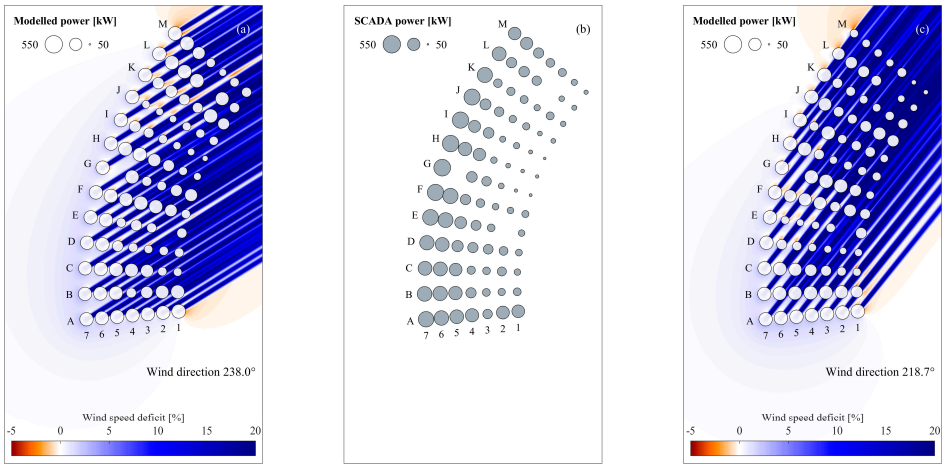

Figure 11. (**a**) Simulation of wakes and blockage showing the wind speed deficit in percentage (colors). The sizes of the circles indicate the modeled power at every turbine. The wind direction was from the wind lidar data, and the inflow wind speed was derived from unwaked front−row turbines. (**b**) Measured power production at each turbine at Horns Rev 2 offshore wind farm on 16 April 2018 at 15:10 UTC, indicated by the size of the circles. Three turbines did not produce (missing circles). (**c**) Same as (**a**) but for the wind direction estimated near the surface.

The model results predicted blockage effects in an arc curve in the local area upwind south and west of the wind farm, see Figure 11a. The fog in the photographs was located approximately in the same local area. In areas with lower winds (stagnant air), condensation processes could be the causal reason for the warm, moist air transforming to fog. The condensation is dependent upon a delicate balance between humidity, temperature, and air movements. Higher winds will dissolve the fog. Thus, the areal extent of the fog is likely to reveal the low wind speed region.

The measured production per turbine at 15:10 UTC is shown in Figure 11b. All but three turbines produced power. Some produce below 100 kW, most between 100 and 400 kW, and few above 400 kW. The turbines with the highest production are located along the western front row. The large variation in power production is due to wind speeds just above cut-in and the wake effects.

The wind speed deficit in Figure 11a,c differs slightly in the upwind area affected by the blockage effect as well as accelerated flow along the sides of the wind farm and between turbines. As already said, the power production compared best in Figure 11a based on the wind direction at hub height, while the fog trails were better matched in Figure 11c with wind direction near the surface. The slightly accelerated flow from between

turbines is present in both Figure 11a,c and is expected to be more pronounced closer to the surface than at hub height. The accelerated flow below and between turbines is due to the deflection of some air mass below the turbine rotors. This has been observed at wind farms offshore in SAR [11,32] and wind farms on land by lidar [33] and modeled by WRF [14] and LES [34]. The accelerated flow would explain the overall dominant clearing of sea fog near the surface between the turbines, as visible in the photos.

The production of power at the Horns Rev 2 offshore wind farm on 16 April 2018 from 6:00 to 24:00 is shown in the form of the normalized park total power in Figure 12. At the time of the photographs, the normalized park total power was 10% of the installed capacity.

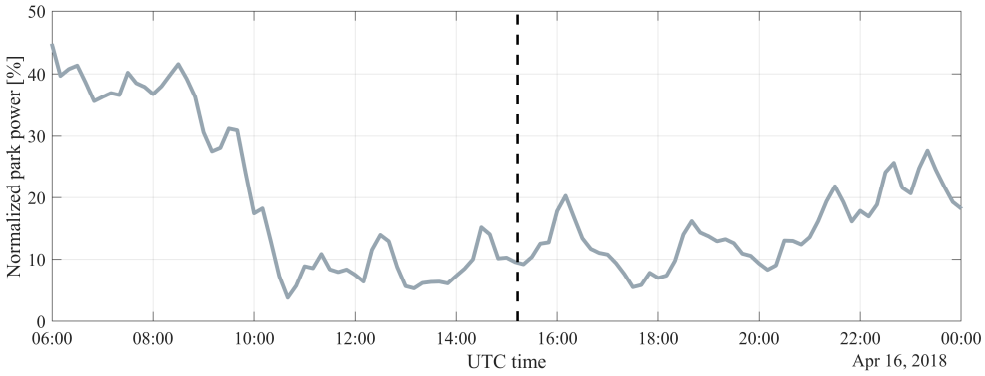

Figure 12. Park total power normalized with rated power (91 × 2300 kW = 209.3 MW) from SCADA at Horns Rev 2 offshore wind farm on 16 April 2018. The time of the photographs is indicated with the dashed line.

5. Discussion

At the time of the photos, the local ambient meteorological conditions at Horns Rev were characterized by wind speed around 6 m s^{-1} at hub height, wind direction from SW, a shallow boundary layer, stable stratification, a strong veer, low turbulence, and high relative humidity. Advection of warm and moist air mass over the cool sea caused cold sea fog. This is supported by satellite, lidar, and meteorological observations and reanalysis model results. Stable stratification is frequently observed during spring at Horns Rev [35]. 16 April is in the midst of this season.

The Horn Rev 2 wind farm produced 10% of rated power at the time of the photos. The highest power production was at the turbines located on the western edge, while turbines in the deep array produced very little due to the low winds near cut-in. Results from the engineering wake and blockage model of Horns Rev 2 predict a strong velocity deficit in the downwind area, around 10% to 20% velocity deficit. This corresponds to low power production as the turbine cut-in wind speed is 4 m s^{-1}. In stable stratification, wakes are long and narrow as the mixing process is suppressed. Long and narrow wakes are observed in the photos. The wakes reach from one turbine to the next without much widening. There was a clockwise rotation due to a strong veer. The foggy wakes most likely were caused by the upward movement of humid air condensing in the wakefield where the dew point temperature was reached, a process previously supported by LES modeling of the wake dynamics in stable conditions with a shallow cold fog layer in the photo case in January 2016 [20].

Looking at the far end of the wind farm, a clearing of the foggy wakes is noticed at the last few rows of turbines and beyond. A plausible cause for the fog dissolving in this region could be due to the entrainment of drier air from aloft mixing down into the shallow boundary layer. A similar entrainment effect was explained to clear the fog downstream of the wind farm in the photo case in January 2016 [20]. For that case, the entrainment process was modeled from a mesoscale model, including an explicit parametrization of the wind farm effect on the atmospheric flow, and the entrainment drying effect was predicted to

reach many kilometers downstream [20], which also appears to be present in the photo case from 16 April 2018 as the clearing stretches far downstream.

Four hours before the photos, a Sentinel-2 image from the European Space Agency observed at 10:53:33 UTC over DanTysk and Sandbank wind farms southwest of Horns Reef showed visible wakes [36]. Sentinel-1 is an optical sensor, and the "true color" image shows bright clouds, darker seas, and, in light gray, the complex wake structures in DanTysk and Sandbank. This is likely due to cold sea fog in this area, but it is outside our study area and scope. Horns Rev was covered in clouds at this time.

Moving on to study the blockage effect at Horns Rev, the engineering model predicted a large arc shape region upwind SW of the wind farm. The velocity deficit due to blockage was much smaller than the wake velocity deficit. This corresponds well with other model studies on blockage and wake velocity deficit [1–5]. The reduced wind speed of 1% extended around 1000 m, or around 10D. Closer to the wind farm, a higher velocity deficit of up to 2% was predicted. The model results were for hub-height winds. Blockage and wake effects depend upon turbine layout, size and spacing of turbines, and their operation [4,5,13,33]. For turbines in closely spaced grid layouts, more pronounced wake effects were found than for curved layouts [37]. Horns Rev 2 with a curved layout is expected to have less wake loss and lower blockage effect than wind farms in grid layout.

The variation of the blockage effect with vertical distance from surface to hub height needs consideration. CFD model results suggest a rather constant blockage effect from surface to hub height [1]. Furthermore, analysis of meteorological mast data near a wind farm showed only small variations in blockage effect comparing between 70% of hub height versus hub height [1] and analysis of lidar observations at 25 m for a wind farm with turbines hub height at 92 m, i.e., 27% of hub height, showed blockage effects of 4% at a distance of 25D (2.9 km) in stable conditions offshore [18]. From visual inspection of the photos, the cold sea fog horizontally stretches ~ 1000 m upstream, i.e., ~10D, south of the wind farm, and ~2000 m, i.e., ~20D, west of the wind farm. The cold sea fog reached a vertical extent slightly below the lower tip height (21.5 m). This corresponds to heights less than 30% of hub height.

Turbines operating in the partial load range and stable stratification appear to cause reduced winds far upstream ~20 D or more from scanning lidar data analysis [18] and from visual inspection of the fog in the current case. The blockage effect has a long horizontal extent.

As mentioned in the introduction, fog formation is governed by the moisture–temperature structure, wind speeds, wind shear, mixing processes, and turbulence intensity. From the analysis, it can be assumed that the wind speeds were some percentage lower upstream due to the blockage effect. Lower winds in the area, possibly affected by wind farm blockage, might explain the fog condensation. Fog tends to form in low winds, while higher winds tend to thwart condensation. In the SW corner of the wind farm, winds may be slightly higher, and the blockage is only weak; therefore, we do not see fog condensation in this region. This might be ascribed to spatial inhomogeneity in the flow locally.

At the time of the photos, a strong veer was present. Data from the wind lidar shows a veer at 0.14°/m in the upper swept rotor area, and using a combination of lidar and ASCAT, a possible veer at 0.48°/m (or less) was inferred in the lower rotor swept area and down to the surface. Comparing this extraordinarily strong veer to other studies reveals it is not unrealistic. LES model simulation of the blockage effect showed the strongest veer for very stable conditions [5,38]. Observations of winds at 10 m and 116 m height at a mast in Texas, US, showed veer in stable conditions with values slightly above 0.4°/m at the extreme end of the distribution [39]. Furthermore, [40] reported meteorological mast observations from 10 m and 98 m height with a veer at 30°/m for a shallow stable nocturnal boundary layer on land. At the coastal site, Høvsøre, 55 km north of Hvide Sande, wind profile lidar data showed a strong veer in stable conditions [41,42]. Also, offshore data supported strong veer to exist. According to [43] observations at 40 m and 200 m height at the US East Coast

documented veer to reach 0.4°/m based on lidar observations. It is realistic that a strong veer was present from the surface and within the rotor-swept area. In general, strong veer reduces AEP compared to winds with negligible veer. An indication of the veer is the clockwise turning of the wakes at Horns Rev seen in the photos.

6. Conclusions

Our study aim was to investigate whether wind farm blockage is a likely cause for the observed fog formation. The approach is novel. Our study is the first on offshore wind farm blockage effect revealed by fog.

The foggy conditions in the photos from 16 April 2018 visually outlined an area with shallow sea fog upwind of the Horns Rev 2 wind farm. The area extent reached ~10D south and ~20 D west upstream of the wind farm.

It is the first time a visual imprint of the blockage effect has become visible due to fog formation in the reduced wind speed area upwind of a wind farm.

Analysis of the ambient meteorological conditions and results from an engineering wake and blockage model for the wind farm supported the idea that a blockage effect might occur. The atmosphere was stably stratified with winds around 6 m s^{-1} at hub height, wind direction from SW, and a warm, moist air mass over a cooler sea. The precursor for cold fog formation is present with such ambient conditions, and sea fog could materialize when the wind speed is sufficiently low. Reduced wind speed upstream ~10 D south and ~20 D west of the wind farm could be caused by blockage, and therefore, blockage could have triggered the fog formation.

Wind farm wakes were long and narrow, as visually seen in the photos, and predicted by the wake model for stable stratification. Clockwise turning of the wakes was ascribed to veer in the rotor-swept area and below.

In conclusion, based on the available meteorological observations and results from an engineering wake and blockage model, it is plausible that the fog revealed a blockage effect at the Horns Rev 2 wind farm.

The implications of the study for researchers could include a comparison to LES modeling, adding atmospheric stability and veering to the flow equations to achieve results on the blockage and wind farm wake effects with greater detail near the wind farm. WRF modelers could use and test wind farm parametrizations to capture the formation of fog as well as the blockage effect, wind farm wake, and entrainment at the far field for the case. Wind farm developers and operators could gain further insight into flow phenomena at large offshore wind farms, such as blockage upstream and veering of the wake.

Author Contributions: C.B.H. wrote the paper; N.G.N. analyzed data for Figures 1 and 6–12 and prepared the graphics; G.S.P. discussed the results. All authors have read and agreed to the published version of the manuscript.

Funding: This research received no external funding.

Data Availability Statement: Lidar and wind farm operational data are from Ørsted. Satellite SST data are from GHRSST, DMI, and MyOcean regional data assembly center. Meteorological data from Hvide Sande are from DMI. ASCAT data are from NOAA NESDIS. The cloud cover map is from Sat24.com/Eumetsat/Met office. ERA5 data are from ECMWF. FINO3 data was made available by the FINO (Forschungsplattformen in Nord- und Ostsee) initiative, which was funded by the German Federal Ministry of Economic Affairs and Climate Action (BMWK) on the basis of a decision by the German Bundestag, organized by the Projekttraeger Juelich (PTJ) and coordinated by the German Federal Maritime and Hydrographic Agency (BSH).

Acknowledgments: We acknowledge all data used. The photographs are from helicopter pilot Henrik Krogh.

Conflicts of Interest: Author Nicolai Gayle Nygaard was employed by the Ørsted A/S. Author Gregory S. Poulos was employed by the ArcVera Renewables. The remaining author declares that the research was conducted in the absence of any commercial or financial relationships that could be construed as a potential conflict of interest.

References

1. Bleeg, J.; Purcell, M.; Ruisi, R.; Traiger, E. Wind Farm Blockage and the consequences of Neglecting Its Impact on Energy Production. *Energies* **2018**, *11*, 1609. [CrossRef]
2. Branlard, E.; Meyer Forsting, A.R. Assessing the blockage effect of wind turbines and wind farms using an analytical vortex model. *Wind Energy* **2020**, *23*, 2068–2086. [CrossRef]
3. Branlard, E.; Quon, E.; Forsting, A.R.M.; King, J.; Moriarty, P. Wind farm blockage effects: Comparison of different engineering models. *J. Phys. Conf. Ser.* **2020**, *1618*, 062036. [CrossRef]
4. Strickland, J.M.I.; Stevens, R.J.A.M. Investigating wind farm blockage in a neutral boundary layer using large-eddy simulations. *Eur. J. Mech. B Fluids* **2022**, *95*, 303–314. [CrossRef]
5. Strickland, J.M.I.; Gadde, S.N.; Stevens, R.J.A.M. Wind farm blockage in a stable atmospheric boundary layer. *Renew. Energy* **2022**, *197*, 50–58. [CrossRef]
6. Allaerts, D.; Meyers, J. Gravity Waves and Wind-Farm Efficiency in Neutral and Stable Conditions. *Bound. Layer Meteorol.* **2018**, *166*, 269–299. [CrossRef] [PubMed]
7. Allaerts, D.; Meyer, J. Sensitivity and feedback of wind-farm-induced gravity waves. *J. Fluid Mech.* **2019**, *862*, 990–1028. [CrossRef]
8. Lanzilao, L.; Meyers, J. Set-point optimization in wind farms to mitigate effects of flow blockage induced by atmospheric gravity waves. *Wind Energy Sci.* **2021**, *6*, 247–271. [CrossRef]
9. Wu, K.L.; Porté-Agel, F. Flow adjustment inside and around large finite-size wind farms. *Energies* **2017**, *10*, 2164. [CrossRef]
10. Christiansen, M.B.; Hasager, C.B. Using airborne and satellite SAR for wake mapping offshore. *Wind Energy* **2006**, *9*, 437–455. [CrossRef]
11. Djath, B.; Schulz-Stellenfleth, J.; Canadillas, B. Impact of atmospheric stability on X-band and C-band Synthetic Aperture Radar imagery of offshore windpark wakes. *J. Substain. Renew. Energy* **2018**, *10*, 043301. [CrossRef]
12. Nygard, N.G.; Hansen, S.D. Wake effects between two neighbouring wind farms. *J. Phys. Conf. Ser.* **2016**, *753*, 032020. [CrossRef]
13. Owda, A.; Badger, M. Wind Speed Variation Mapped Using SAR before and after Commissioning of Offshore Wind Farms. *Remote Sens.* **2022**, *14*, 1464. [CrossRef]
14. Larsén, X.G.; Fischereit, J. A case study of wind farm effects using two wake parameterizations in the Weather Research and Forecasting (WRF) model (V3.7.1) in the presence of low-level jets. *Geosci. Model Dev.* **2021**, *14*, 3141–3158. [CrossRef]
15. Jacquet, C.; Apgar, D.; Chauchan, V.; Storey, R.; Kern, S.; Davoust, S. Farm blockage model validation using pre and post construction LiDAR measurements. *J. Phys. Conf. Ser.* **2022**, *2265*, 022009. [CrossRef]
16. Sebastiani, A.; Castellani, F.; Crasto, G.; Segalini, A. Data analysis and simulation of the Lillgrund wind farm. *Wind Energy* **2021**, *24*, 634–648. [CrossRef]
17. Nygaard, N.G.; Steen, S.T.; Poulsen, L.; Pedersen, J.G. Modelling cluster wakes and wind farm blockage. *J. Phys. Conf. Ser.* **2020**, *1618*, 062072. [CrossRef]
18. Schneemann, J.; Theuer, F.; Rott, A.; Dörenkämper, M.; Kühn, M. Offshore wind farm global blockage measured with scanning lidar. *Wind Energy Sci.* **2021**, *6*, 521–538. [CrossRef]
19. Hasager, C.B.; Rasmussen, L.; Peña, A.; Jensen, L.E.; Réthoré, P.-E. Wind Farm Wake: The Horns Rev Photo Case. *Energies* **2013**, *6*, 696–716. [CrossRef]
20. Hasager, C.B.; Nygaard, N.G.; Volker, P.J.H.; Karagali, I.; Andersen, S.J.; Badger, J. Wind Farm Wake: The 2016 Horns Rev Photo Case. *Energies* **2017**, *10*, 317. [CrossRef]
21. Koračin, D.; Dorman, C.E.; Lewis, J.M.; Hudson, J.G.; Wilcox, E.M.; Torregrosa, A. Marine fog: A review. *Atmos. Res.* **2014**, *143*, 142–175. [CrossRef]
22. Hancock, P.E.; Zhang, S.; Pascheke, F.; Hayden, P. Wind tunnel simulation of a wind turbine wake in neutral, stable and unstable wind flow. *J. Phys. Conf. Ser.* **2014**, *555*, 01204. [CrossRef]
23. Sat24.com/Eumetsat/Met Office. Available online: https://en.sat24.com/en (accessed on 20 October 2023).
24. Høyer, J.L.; She, J. Optimal interpolation of sea surface temperature for the North Sea and Baltic Sea. *J. Mar. Syst.* **2007**, *65*, 176–189. [CrossRef]
25. NOAA NESDIS. Available online: https://manati.star.nesdis.noaa.gov/datasets/ASCATData.php (accessed on 20 October 2023).
26. Gottschall, J.; Courtney, M.S.; Wagner, R.; Jørgensen, H.E.; Antoniou, I. Lidar profilers in the context of wind energy—A verification procedure for traceable measurements. *Wind Energy* **2012**, *15*, 147–159. [CrossRef]
27. BSH. Available online: https://www.bsh.de/EN/TOPICS/Monitoring_systems/MARNET_monitoring_network/FINO/fino_node.html (accessed on 20 October 2023).
28. ERA5 Hourly Data on Single Levels from 1979 to Present. Copernicus Climate Change Service (C3S) Climate Data Store (CDS). Available online: https://cds.climate.copernicus.eu/cdsapp#!/dataset/reanalysis-era5-single-levels?tab=overview (accessed on 20 October 2023).
29. Hersbach, H.; Bell, B.; Berrisford, P.; Hirahara, S.; Horányi, A.; Muñoz-Sabater, J.; Nicolas, J.; Peubey, C.; Radu, R.; Schepers, D.; et al. The ERA5 global reanalysis. *Q. J. R. Meteorol. Soc.* **2020**, *146*, 1999–2049. [CrossRef]
30. Hatfield, D.; Hasager, C.B.; Karagali, I. Comparing Offshore Ferry Lidar Measurements in the Southern Baltic Sea with ASCAT, FINO2 and WRF. *Remote Sens.* **2022**, *14*, 1427. [CrossRef]
31. Van der Laan, M.P.; Sørensen, N.N. Why the Coriolis force turns a wind farm wake clockwise in the Northern Hemisphere. *Wind Energy Sci.* **2017**, *2*, 285–294. [CrossRef]

32. Platis, A.; Siedersleben, S.K.; Bange, J.; Lampert, A.; Bärfuss, K.; Hankers, R.; Cañadillas, B.; Foreman, R.; Schulz-Stellenfleth, J.; Djath, B.; et al. First in situ evidence of wakes in the far field behind offshore wind farms. *Sci. Rep.* **2018**, *8*, 2163. [CrossRef] [PubMed]
33. Bodini, N.; Lundquist, J.K.; Moriarty, P. Wind plants can impact long-term local atmospheric conditions. *Sci. Rep.* **2021**, *11*, 22939. [CrossRef]
34. Yang, D.; Meneveau, C.; Shen, L. Large-eddy simulation of offshore wind farm. *Phys. Fluids* **2014**, *26*, 025101. [CrossRef]
35. Sathe, A.; Gryning, S.-E.; Pena, A. Comparison of the atmospheric stability and wind profiles at two wind farm sites over a long marine fetch in the North Sea. *Wind Energy* **2011**, *14*, 767–780. [CrossRef]
36. Sentinel-2 Image. Available online: https://sentinelshare.page.link/4WHj (accessed on 20 October 2023).
37. Nygaard, N.G. Wakes in very large wind farms and the effect of neighbouring wind farms. *J. Phys. Conf. Ser.* **2014**, *524*, 012162. [CrossRef]
38. Abkar, M.; Sharifi, A.; Porté-Agel, F. Wake flow in a wind farm during a diurnal cycle. *J. Turbul.* **2016**, *17*, 420. [CrossRef]
39. Walter, K.; Weiss, C.C.; Swift, A.H.P.; Chapman, J.; Kelley, N.D. Speed and direction shear in the stable nocturnal boundary layer. *J. Sol. Energy Eng.* **2009**, *131*, 0110131. [CrossRef]
40. Giebel, G.; Gryning, S.-E. Shear and stability in high met masts, and how WAsP treats it. In Proceedings of the EWEA Special Topic Conference: The Science of Making Torque from Wind, Delft, The Netherlands, 19–21 April 2004; The European Wind Energy Association: Brussels, Belgium, 2004; pp. 356–363.
41. Peña, A.; Floors, R.; Gryning, S.E. The Høvsøre Tall Wind-Profile Experiment: A Description of Wind Profile Observations in the Atmospheric Boundary Layer. *Bound. Layer Meteorol.* **2014**, *150*, 69–89. [CrossRef]
42. Peña, A.; Gryning, S.E.; Floors, R. The turning of the wind in the atmospheric boundary layer. *J. Phys. Conf. Ser.* **2014**, *524*, 012118. [CrossRef]
43. Bodini, N.; Lundquist, J.K.; Kirincich, A.U.S. East Coast lidar measurements show offshore wind turbines will encounter very low atmospheric turbulence. *Geophys. Res. Lett.* **2019**, *46*, 5582. [CrossRef]